Pergamon

Cement and Concrete Research 32 (2002) 647–655

CEMENT AND CONCRETE RESEARCH

Phase separation induced by hydration of the mixed Ca/Sr aluminates $Ca_{3-x}Sr_xAl_2O_6$ A crystallographic study

Anti K. Prodjosantoso[a,b], Brendan J. Kennedy[a,*], Brett A. Hunter[c]

[a]*School of Chemistry, University of Sydney, Sydney, NSW 2006, Australia*
[b]*Jurusan Kimia, Universitas Negeri Yogyakarta, Yogyakarta, DIY 55281, Indonesia*
[c]*Australian Nuclear Science and Technology Organisation, Private Mail Bag 1, Menai, NSW 2234, Australia*

Received 11 July 2001; accepted 12 November 2001

Abstract

The compounds formed by the hydration of single-phase samples of the mixed, solid solution, Ca/Sr aluminates, $Ca_{3-x}Sr_xAl_2O_6$, $3 \leq x \leq 0$ have been studied using high-resolution synchrotron powder diffraction. Hydration of these mixed metal aluminates generally resulted in the formation of at least two hydrogarnet phases, one Ca-rich and the other Sr-rich. The structures of these hydrogarnets have been refined from neutron or synchrotron powder X-ray diffraction (XRD) data. A simple solubility model to explain the phase separation is presented.

Keywords: Crystal structure; X-ray diffraction; $Ca_3Al_2O_6$; Sr

1. Introduction

Tricalcium aluminate ($Ca_3Al_2O_6$) is one of the main phases in ordinary Portland cements. It forms solid solutions with various metal oxides, including Cr, Fe, Mg, Na, Cr, Sr and Ba [1]. The ionic substitutions in this phase can induce some modifications in the structure, reactions and properties. $Ca_3Al_2O_6$ is very stable in dry air [2], but it reacts spontaneously with water forming a range of complex hydroxides, the precise identity of which depends on the hydration temperature [3,4]. Below 15 °C, the main hydrate phase formed is $CaAl_2O_4{\cdot}10H_2O$, while between 15 and 30 °C, both $Ca_2Al_2O_5{\cdot}8H_2O$ and $Al(OH)_3$ are formed. On standing, both calcium aluminate hydrates, $CaAl_2O_4{\cdot}10H_2O$ and $Ca_2Al_2O_5{\cdot}8H_2O$, transform to the thermodynamically stable hydrogarnet $Ca_3Al_2(O_4H_4)_3$. At temperatures above 30 °C, $Ca_3Al_2(O_4H_4)_3$ and $Al(OH)_3$ crystallise [5,6].

There is currently considerable interest in using various low-grade waste materials, such as fly ash, as low-cost raw materials in the production of Portland cement [7]. Fly ash contains a wide variety of trace elements including varying amounts of Sr. Strontium has been reported as a relatively minor constituent of cement [8] and it may be expected to be present in various strontium–calcium aluminates. Formation of the Ca hydrogarnet, $Ca_3Al_2(O_4H/D_4)_3$, is slower than that of the corresponding Sr compound, $Sr_3Al_2(O_4H/D_4)_3$ [5], indicating that $Sr_3Al_2O_6$ is more reactive than $Ca_3Al_2O_6$. Chakoumakos et al. [9] suggested two possible reasons for the increased reactivity of $Sr_3Al_2O_6$ relative to $Ca_3Al_2O_6$. Firstly, the increased size of the Sr cations increases the size of the channels within the Al_6O_8 rings allowing for more rapid diffusion of water [5]. Secondly, there is considerable overbonding at three of the Sr cation sites suggesting that there is considerable strain in $Sr_3Al_2O_6$ that is relieved upon reaction. The incorporation of Sr into Portland cement may alter the properties of the cement formed upon reaction with water.

Despite numerous studies of the structures of the various hydrates in Portland cements, only the structure of hydrogarnet $Ca_3Al_2(O_4H_4)_3$ has been well established [6]. Interestingly, $Sr_3Al_2(O_4H_4)_3$ is isostructrural with $Ca_3Al_2(O_4H_4)_3$, both having a cubic structure $a \approx 15$ Å in space group *Ia3d* [9]. The structures of deuterated analogues have also been studied using neutron powder diffraction methods to accur-

* Corresponding author. Tel.: +61-2-9351-2742; fax: +61-2-9351-3329.
E-mail address: b.kennedy@chem.usyd.edu.au (B.J. Kennedy).

0008-8846/02/$ – see front matter
PII: S0008-8846(01)00737-2

ately determine the location of the D(H) atoms [6,9]. These studies have suggested that the O–D groups remain 'free' and exist in $Al(OD)_6$ polyhedra. The O–D bond length was found to be ~ 0.95 Å.

It is well known that although Sr^{2+} is larger than Ca^{2+} (1.13 vs. 0.99 Å), Sr can partially replace Ca in numerous metal oxides, and a number of studies of mixed Ca/Sr aluminates have been repeated [8,10–12]. These and other studies have shown that it is often possible to synthesise single-phase mixed oxides. Despite the importance of Ca aluminates in Portland cement and the potential incorporation of impurity cations such as Sr, there are few systematic studies on the effect of substitution on the hydration properties. Using powder X-ray diffraction (XRD) methods, Carlson [8] reported that hydrothermal reaction of $Ca_{3-x}Sr_xAl_2O_6$ ($x = 2.75$, 2.5 and 2.25) at 160 °C produces two separate species, one apparently rich in calcium and the other rich in strontium. We are unaware of any subsequent detailed studies on this phenomenon. In the present work, we have investigated the hydration of a comprehensive series of oxides of the type $Ca_{3-x}Sr_xAl_2O_6$ and characterised the resulting crystalline phases using powder diffraction methods. In selected cases, the oxides were deuterated and the structures investigated using neutron diffraction.

2. Experimental

2.1. Sample preparation

Samples of $Ca_{3-x}Sr_xAl_2O_3$ were prepared using the method described by Prodjosantoso et al. [11]. Hydrated or deuterated samples were prepared by adding H_2O or D_2O to the finely powdered oxides in the mole ratio of 100:1. The mixtures were stirred for 1 day, 3 days, 1 week or 2 weeks under a nitrogen atmosphere. The reactions were terminated by addition of acetone, and the solids were collected by filtration and then dried under a stream of dry nitrogen. The samples were then characterised using powder XRD and synchrotron XRD and, for deuterated samples, neutron diffraction.

2.2. X-ray, synchrotron X-ray and neutron diffraction

X-ray powder diffraction patterns were collected in the range of $2\theta = 5–90°$, step size of 0.02° and counting time 10 s per step using a Siemens D-5000 Diffractometer (40 kV, 20 mA, with divergence and antiscatter slits 1 mm, receiver slit 0.2 mm and detector slit 0.6 mm), using CuKα radiation ($\lambda = 1.5406$ Å). In order to obtain higher resolution diffraction patterns, synchrotron powder XRD data were collected at room temperature on the Australian National Beamline Facility (ANBF) at the KEK Photon Factory, Tsukuba, Japan. Samples were mounted in 0.5-mm diameter glass capillaries. The wavelength of the measurements, 0.99702 Å, was determined using an NIST Si 640b standard. Diffraction patterns were recorded using three image plates as detectors over the angular range of $2\theta = 5–45°$, 45–85° and 85–125°. The neutron diffraction patterns were collected on the High Resolution Powder Diffractometer (HPRD) at the HIFAR facility at the ANSTO Lucas Heights Research Laboratories. Samples were housed in 16-mm vanadium cans and these were rotated about the vertical axis to minimise effects due to preferred orientation. Data were collected at room temperature using neutrons of wavelength $\lambda = 1.4925$ or 1.8845 Å between the angles of $2\theta = 10–156°$ and a step size of $2\theta = 0.05°$. Neutron diffraction has the advantage that the scattering length of the elements varies randomly and it affords greater sensitivity to the crystallographic parameters for the lighter D and O atoms.

Structures were refined by the Rietveld method [13], using the program LHPM [14] operating on a personal computer. The Rietveld method is primarily a method of refining crystal structures from powder diffraction data. The pattern calculated from a starting crystallographic model containing information on the space group symmetry, atomic position, site occupancies and lattice parameters is compared to the observed diffraction pattern and by vari-

Table 1
The final refined structural parameter for $Ca_{2.5}Sr_{0.5}Al_2(O_4H/D_4)_3$

	$Ca_{2.5}Sr_{0.5}Al_2(O_4H/D_4)_3$				$Ca_{0.5}Sr_{2.5}Al_2(O_4H/D_4)_3$							
	$a = 12.6239(3)$ Å, $R_{Bragg} = 2.39\%$,				Phase 1 = 60(5) mol% $a = 12.9633(7)$ Å, $R_{Bragg} = 1.51\%$,				Phase 2 = 40(7) mol% $a = 12.9184(10)$ Å, $R_{Bragg} = 1.02\%$			
	$R_p = 3.18\%$, $R_{wp} = 4.06\%$, $R_{exp} = 1.91$, GOF = 4.53				$R_p = 2.54\%$, $R_{wp} = 3.10\%$, $R_{exp} = 2.21$, GOF = 1.96							
Atom	x	y	z	B (Å^2)	x	y	z	B (Å^2)	x	y	z	B (Å^2)
Ca	0	0.25	0.125	1.25(7)	0	0.25	0.125	0.93(8)	0	0.25	0.125	1.1(3)
Sr	0	0.25	0.125	1.25(7)	0	0.25	0.125	0.93(8)	0	0.25	0.125	1.1(3)
Al	0	0	0	0.6(1)	0	0	0	0.9(1)	0	0	0	0.2(3)
O	−0.0263(2)	0.0513(1)	0.1394(1)	1.17(5)	−0.0278(2)	0.0494(2)	0.1362(2)	1.15(7)	−0.0268(9)	0.0507(6)	0.1372(6)	1.8(2)
H[a]	−0.0951(3)	0.0457(2)	0.1570(1)	5.1(1)	−0.0959(5)	0.0382(4)	0.1528(4)	4.1(1)	−0.092(2)	0.057(2)	0.146(2)	5.3(8)
D[a]	−0.0951(3)	0.0457(2)	0.1570(1)	5.1(1)	−0.0959(5)	0.0382(4)	0.1528(4)	4.1(1)	−0.092(2)	0.057(2)	0.146(2)	5.3(8)

In the refinement the APD parameters of the atoms occupy the same site, in the two phases, were constrained be equal.

[a] The n values for H and D in $Ca_{2.5}Sr_{0.5}Al_2(O_4H/D_4)_3$ are 90.0(6) and 6.0(6), respectively. While in $Ca_{0.5}Sr_{2.5}Al_2(O_4H/D_4)_3$ are 81.8(9) and 14.2(9), and 72(4) and 24(4) for Phase 1 and Phase 2, respectively.

ation of the various parameters, optimal agreement between the observed and calculated patterns is obtained. When more than one crystalline phase is present, the scale factors afford quantitative phase information. In the present work, the background in the neutron diffraction patterns was taken to be a quadratic function in 2θ, and this was refined simultaneously with the unit-cell, zero-point, scale, peak width/shape asymmetry and structural parameters. An interpolated background was used in the analysis of the synchrotron diffraction data. The peak profile was described by Voigt function, in which the widths of the Gaussian and Lorentzian components were modelled the instrumental resolution and strain broadening, and with secθ describing crystallite size broadening, respectively.

2.3. Structural refinements

Two representative samples, $Ca_{3-x}Sr_xAl_2(O_4H_4)_3$, $x=0.5$ and 2.5, were deuterated and their structures investigated using powder neutron diffraction methods. The neutron scattering lengths used in the refinements were, for Ca, Sr, Al, O, H and D = 0.4900, 0.7020, 0.3449, 0.5803, −0.3739 and 0.6671 fm, respectively [15]. The diffraction pattern for $Ca_{2.5}Sr_{0.5}Al_2(O_4D_4)_3$ could be successfully fitted using a single-phase model, however, the neutron diffraction data for the $x=2.5$ sample showed the presence of two hydrogarnet-type structures.

For the $x=0.5$ sample, the refinement was commenced using the structural parameters reported by Chakoumakos et al. [9] for pure $Sr_3Al_2(O_4D_4)_3$. The Ca and Sr are disordered at the same atomic position; the asymmetric unit of $Ca_{2.5}Sr_{0.5}Al_2(O_4D_4)_3$ consists of four atoms. The structure was refined to $R_p=3.18\%$, $R_{wp}=4.06\%$, $R_{Bragg}=2.39\%$ and GOF = 4.53 using 24 parameters including positional, profile and background parameters. A summary of the refined structural parameters is listed in Table 1, while selected atomic distances and angles are listed in Table 2. The lattice parameter is $a=12.6239(3)$ Å. The refined H/D content in the deuterated sample is 6.2(4)% H and 93.8(4)% D.

The structures in the $x=2.5$ sample were refined using the $x=0.5$ results as a starting model. The structures were refined to $R_p=2.54\%$, $R_{wp}=3.10\%$, $R_{Bragg}=1.51\%$ and 1.02%, and GOF = 1.96. The model contains two phases,

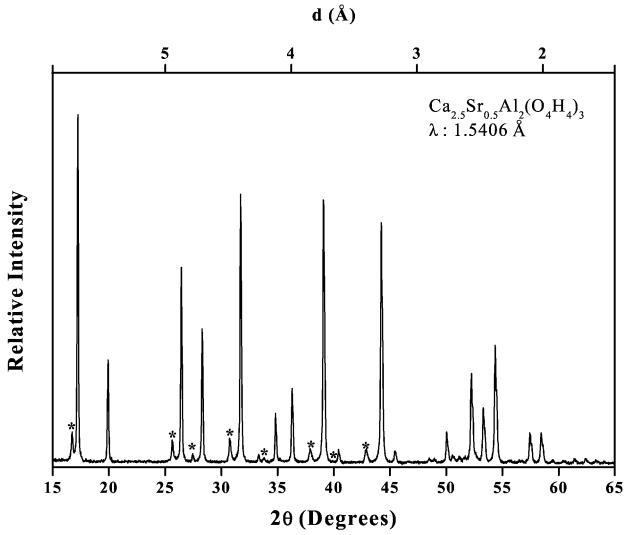

Fig. 1. Powder XRD pattern of $Ca_{2.5}Sr_{0.5}Al_2(O_4H_4)_3$ recorded using CuKα radiation. The peaks labelled * indicate the presence of the second phase $Ca_{3-x}Sr_xAl_2(O_4H_4)_3$ ($x\approx 3$).

Table 2
Selected atomic distances and angles in $Ca_{2.5}Sr_{0.5}Al_2(O_4H/D_4)_3$

	$Ca_3Al_2(O_4D_4)_3$[6]	$Ca_{2.5}Sr_{0.5}Al_2(O_4H/D_4)_3$	$Ca_{0.5}Sr_{2.5}Al_2(O_4H/D_4)_3$ Phase 1	$Ca_{0.5}Sr_{2.5}Al_2(O_4H/D_4)_3$ Phase 2	$Sr_3Al_2(O_4D_4)_3$[9]
Octahedron					
Al–O × 6	1.916(2) Å	1.904(2) Å	1.912(2) Å	1.921(2) Å	1.911(1) Å
O(1)–Al–O(4) × 6	85.6(2)°	84.5(1)°	85.9(1)°	85.0(1)°	86.1(1)°
O(1)–Al–O(5) × 6	94.4(2)°	95.5(1)°	94.1(1)°	95.0(1)°	93.8(1)°
Dodecahedron					
M–O(4) × 4	2.464(2) Å	2.450(2) Å	2.551(3) Å	2.530(3) Å	2.579(2) Å
M–O(4)′ × 4	2.521(2) Å	2.537(2) Å	2.630(3) Å	2.603(3) Å	2.642(1) Å
O(1)–M–O(2) × 2	76.7(1)°	77.80(7)°	77.8(1)°	76.9(1)°	78.4(1)°
O(1)–M–O(4) × 4	62.9(1)°	61.75(7)°	60.4(1)°	60.8(1)°	59.9(1)°
O(1)–M–O(7) × 4	97.1(1)°	97.56(5)°	97.24(8)°	97.61(8)°	97.3(1)°
O(4)–M–O(6) × 4	76.0(1)°	75.91(8)°	78.1(1)°	78.3(1)°	78.1(1)°
O(4)–M–O(7) × 2	73.9(1)°	75.5(1)°	74.5(1)°	74.9(1)°	74.0(1)°
O(7)–M–O(8) × 2	106.8(1)°	105.15(9)°	105.9(1)°	105.5(1)°	108.0(1)°
(O_4D_4) tetrahedral					
O–D × 4	0.906(2) Å	0.903(3) Å	0.920(5) Å	0.857(5) Å	0.914(4) Å
O. . .D					
about O(1)–O(3)	2.567(2) Å	2.610(4) Å	2.800(5) Å	2.639(6) Å	2.697(3) Å
	2.497(2) Å	2.575(4) Å	2.605(5) Å	2.586(6) Å	2.669(3) Å
about O(1)–O(2)	2.959(2) Å	2.977(3) Å	3.182(5) Å	2.997(6) Å	3.109(3) Å

Table 3
The final refined structural parameter for $Ca_{3-x}Sr_xAl_2(O_4H_4)_3$ ($x = 0$ to 3)

x ($Ca_{3-x}Sr_xAl_2(O_4H_4)_3$)	a (Å)	Occupancy of Sr atoms (n observed)	Occupancy of Sr atoms (n theoretical)	% moles	R_p (%)	R_{wp} (%)	R_{exp} (%)	R_{Bragg} (%)	GOF
0	12.5744(2)	0	0	100	6.25	8.48	3.48	1.59	5.94
0.01	12.5719(2)	0.1(1)	0.08	100	5.77	7.58	3.73	1.59	4.14
0.025	12.5716(3)	0.3(2)	0.2	100	7.24	9.96	3.78	1.78	6.93
0.05	12.5709(2)	0.1(1)	0.4	98(2)	6.12	8.12	3.73	1.64	4.73
	13.012(2)	24		1.64(9)				2.86	
0.075	12.5720(2)	0.09(10)	0.6	99(1)	5.58	7.45	3.60	1.67	4.28
	13.017(2)	24		1.13(6)				3.21	
0.1	12.5720(3)	0.2(1)	0.8	98(3)	6.72	9.08	3.35	2.15	7.37
	12.991(1)	24		2.4(1)				4.78	
0.15	12.5796(2)	0.4(1)	1.2	98(2)	7.39	10.29	4.27	2.48	5.80
	13.019(1)	24		1.9(1)				6.59	
0.2	12.5802(3)	0.7(2)	1.6	95(3)	6.64	8.98	3.25	1.38	7.62
	13.0101(3)	24		5(1)				5.65	
0.25	12.5807(2)	0.4(2)	2	96(3)	7.23	9.73	5.43	1.87	3.22
	13.0081(6)	24		4.1(4)				6.83	
0.5	12.6198(3)	2.9(1)	4	96(2)	6.38	8.96	5.06	1.24	3.13
	13.0068(6)	24		4.4(2)				4.89	
1.0	12.674(1)	6.4(4)	8	92.3(4)	8.83	11.75	4.43	2.14	7.04
	13.017(1)	24		7.7(3)				8.94	
1.5	12.7534(2)	7.4(4)	12	79.1(5)	8.69	10.85	4.83	3.77	5.05
	12.8808(2)	5.1(8)		10.4(3)				4.56	
	12.9596(7)	20.9(7)		10.6(3)				4.46	
2	12.839(2)	8.1(4)	16	45(1)	8.46	10.84	4.12	4.04	6.91
	12.933(2)	18(1)		19(1)				3.29	
	12.970(3)	21.3(3)		36(1)				2.80	
2.5	12.944(1)	17.5(5)	20	55(3)	4.21	6.28	3.78	1.80	2.76
	12.9606(7)	20.9(7)		18(1)				2.03	
	13.0267(6)	24		27(1)				1.58	
2.75	13.0022(2)	21.5(4)	22	100	5.39	7.64	2.32	2.16	10.89
2.8	13.0034(5)	22.6(6)	22.4	100	7.19	10.76	3.87	3.39	7.72
2.85	13.0102(3)	23.3(4)	22.8	100	5.16	7.29	4.01	1.82	3.30
2.9	13.0217(3)	23.2(4)	23.2	100	5.83	7.74	2.15	2.29	12.97
2.925	13.0258(2)	23.3(7)	23.4	100	4.90	6.55	2.14	1.93	9.36
2.95	13.0265(3)	23.4(4)	23.6	100	5.35	7.45	2.16	2.50	11.9
2.975	13.0248(2)	23.9(3)	23.8	100	4.91	6.63	2.18	1.95	9.27
2.99	13.0288(2)	24	23.92	100	4.71	6.42	2.19	2.10	8.59
3	13.0351(1)	24	24	100	5.51	7.44	2.37	2.32	9.82

Phase 1 has a lattice parameter of $a = 12.9633(7)$ Å and an abundance of 60(5) mol%, while the minor Phase 2 has $a = 12.9284(10)$ Å and an abundance of 40(5) mol%. For both samples, the refinements provide reasonable views of the geometry of the $Ca(O_4H/D_4)_3$ polyhedra, and established the position of the D atom and hence the O–D distance, as listed in Table 2.

The powder X-ray patterns of $Ca_{3-x}Sr_xAl_2(O_4H_4)_3$ ($x = 2.5$ to 0.5) indicate that at least two different phases of hydrogarnet were present in these samples. For example, the diffraction pattern of a sample of $Ca_{2.5}Sr_{0.5}Al_2O_6$, treated with water, shows the presence of two series of lines demonstrating that two isostructural products are formed (Fig. 1). The position of the lower intensity lines (ca. 5% of the major lines) is similar to that found for pure $Sr_3Al_2(O_4H_4)_3$ (Fig. 1). Subsequently, the structures were refined for 27 samples using synchrotron X-ray powder diffraction data. The samples studied were $Ca_{3-x}Sr_xAl_2(O_4H_4)_3$, where $x = 0.0$, 0.01, 0.025, 0.05, 0.075, 0.1, 0.15, 0.2, 0.25, 0.5, 0.75, 1.0, 1.25, 1.5, 1.75. 2.0, 2.25, 2.5, 2.75, 2.8, 2.85, 2.9, 2.925, 2.95, 2.975, 2.99 and 3.0. The refinements were commenced using the structural parameters of deuterated sample $Ca_{2.5}Sr_{0.5}Al_2(O_4D_4)_3$. The final refined structural parameters are listed in Tables 3 and 4, and selected atomic distances and bond lengths are listed in Table 5. The observed, calculated and difference neutron powder diffraction profiles for $Ca_{2.5}Sr_{0.5}Al_2(O_4H/D_4)_3$ and synchrotron X-ray powder diffraction profiles for $Ca_{2.5}Sr_{0.5}Al_2(O_4H_4)_3$ are shown in Fig. 2.

3. Results and discussion

The powder XRD patterns for the 27 compounds of the type $Ca_{3-x}Sr_xAl_2(O_4H_4)_3$, $0 \le x \le 3$, shown in Fig. 3, clearly illustrates the formation of a second hydrogarnet compound at low x-values, $x > 0.075$ as evidenced from the weak peaks at $2\theta = 16.72°$, 25.72° and 30.82° ($d = 5.2960$,

Table 4
The oxygen positional parameters for the major phase in the series of $Ca_{3-x}Sr_xAl_2(O_4H_4)_3$

	O atom		
x ($Ca_{3-x}Sr_xAl_2(O_4H_4)_3$)	x	y	z
0	−0.0280(2)	0.0521(2)	0.1399(2)
0.01	−0.0280(1)	0.0519(2)	0.1400(2)
0.025	−0.0283(2)	0.0517(2)	0.1401(2)
0.05	−0.0282(2)	0.0522(2)	0.1401(2)
0.075	−0.0284(2)	0.0518(2)	0.1401(2)
0.1	−0.0284(2)	0.0517(2)	0.1404(2)
0.15	−0.0280(1)	0.0518(2)	0.1404(2)
0.2	−0.0275(2)	0.0514(2)	0.1409(3)
0.25	−0.0285(2)	0.0520(2)	0.1404(2)
0.5	−0.0287(1)	0.0515(2)	0.1397(2)
1	−0.0312(3)	0.0505(4)	0.1414(5)
1.5	−0.0329(3)	0.0569(3)	0.1448(5)
2	−0.0298(3)	0.0502(4)	0.1433(4)
2.5	−0.0300(1)	0.0515(2)	0.1398(2)
2.75	−0.0294(2)	0.0489(3)	0.1382(3)
2.8	−0.0297(3)	0.0490(4)	0.1396(4)
2.85	−0.0295(2)	0.0484(3)	0.1376(3)
2.9	−0.0293(2)	0.0488(3)	0.1375(3)
2.925	−0.0286(2)	0.0488(2)	0.1376(2)
2.95	−0.0292(2)	0.0489(3)	0.1380(3)
2.975	−0.0288(2)	0.0487(2)	0.1369(2)
2.99	−0.0289(2)	0.0491(2)	0.1365(2)
3	−0.0297(3)	0.0486(3)	0.1379(3)

For the refined Ca/Si ratios, see Table 3.

3.4596 and 2.8977 Å). In the region $0.1 \leq x \leq 1$, there is a progressive increase in the intensity of these peaks. In the region $0.75 < x < 2.5$, the crystallinity of the samples apparently decreases, while at still higher Sr contents, the crystallinity increases and the samples are single phase. The addition of the larger Sr cations results in a gradual shift in the positions of the Bragg reflections as a result of the increasing size of the lattice parameter.

Table 5
Atomic distances in the $Ca_{3-x}Sr_xAl_2(O_4H_4)_3$

x ($Ca_{3-x}Sr_xAl_2(O_4H_4)_3$)	Al–O (Å)	M–O(4) × 4 (Å)	M–O(4)′ × 4 (Å)
0	1.910(2)	2.459(2)	2.521(2)
0.01	1.910(2)	2.457(2)	2.522(2)
0.025	1.910(3)	2.459(3)	2.525(3)
0.005	1.91(3)	2.460(1)	2.519(6)
0.075	1.91(3)	2.460(7)	2.525(1)
0.1	1.91(4)	2.458(6)	2.526(3)
0.15	1.92(3)	2.456(7)	2.526(9)
0.2	1.92(3)	2.446(3)	2.530(4)
0.25	1.92(4)	2.462(1)	2.524(1)
0.5	1.9(1)	2.474(9)	2.534(9)
1	1.94(6)	2.516(6)	2.540(6)
1.5	2.014(5)	2.535(4)	2.523(4)
2	1.987(5)	2.498(4)	2.604(5)
2.5	1.970(3)	2.554(2)	2.609(2)
2.75	1.944(4)	2.559(3)	2.648(3)
2.8	1.962(5)	2.553(4)	2.649(5)
2.85	1.936(4)	2.565(3)	2.656(3)
2.9	1.938(4)	2.567(3)	2.652(4)
2.925	1.937(3)	2.560(3)	2.653(3)
2.95	1.945(4)	2.562(3)	2.653(3)
2.975	1.930(3)	2.567(3)	2.651(3)
2.99	1.927(3)	2.572(2)	2.649(3)
3	1.945(4)	2.569(4)	2.659(4)

The persistence of the second Sr-rich phases in all the samples could indicate that the starting oxides were multiphasic. A high-resolution synchrotron diffraction pattern of $Ca_{1.5}Sr_{1.5}Al_2O_6$ shows that this oxide is indeed single phase (Fig. 4). It is evident that the hydration reaction results in segregation into the two phases, one Ca-rich and the other Sr-rich.

In order to confirm that the second phase is a hydrogarnet, high-resolution synchrotron diffraction data were collected for all the samples and analysed by the Rietveld method. As is evident from Fig. 2b, the synchrotron profiles were well fitted to a two-phase hydrogarnet model in which the lattice parameter of the minor phase 13.0068(6) Å was very similar to that found for pure

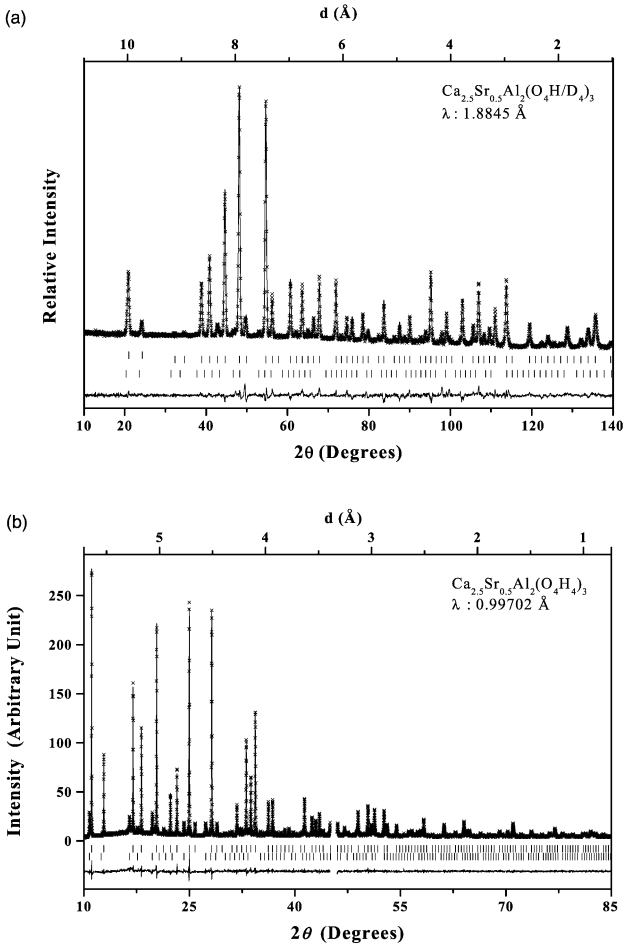

Fig. 2. Observed, calculated and differences diffraction patterns for the (a) neutron powder diffraction of $Ca_{2.5}Sr_{0.5}Al_2(O_4H/D_4)_3$ and (b) synchrotron X-ray powder diffraction data of $Ca_{2.5}Sr_{0.5}Al_2(O_4H_4)_3$. The crosses indicate the observed data points and the solid line is that calculated from a refinement. The short lines below the pattern mark the positions of all Bragg reflections, and the lower curve represents the difference between the observed and calculated patterns.

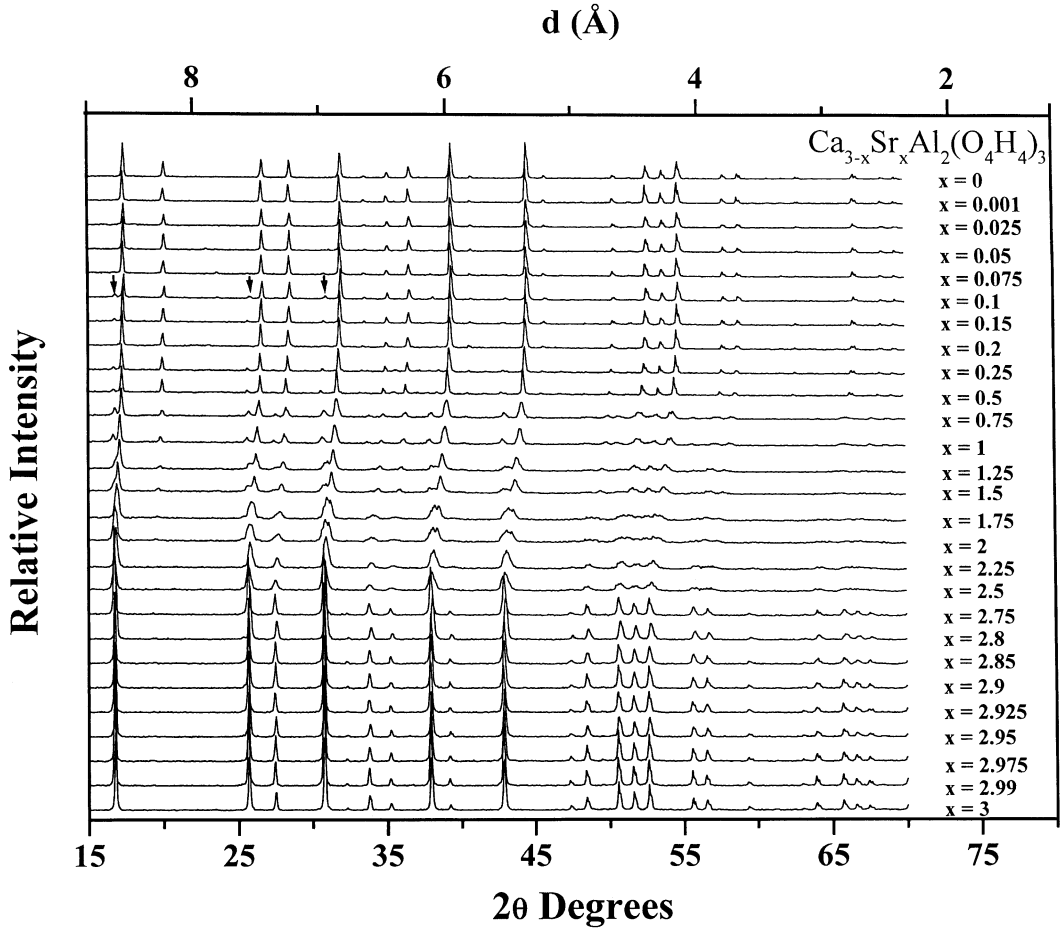

Fig. 3. Powder XRD patterns for the series $Ca_{3-x}Sr_xAl_2(O_4H_4)_3$, collected using CuK$\alpha$ radiation. The arrows near the $x=0.1$ sample highlight the growth of the second hydrogarnet phase.

$Sr_3Al_2(O_4H_4)_3$, 13.0351(1) Å. Surprisingly, it was possible to reproduce the observed neutron diffraction profile for the deuterated compound $Ca_{2.5}Sr_5Al_2(O_4D_4)_3$ using a single-phase model (Fig. 2b). In part, this observation may be related to the lower resolution of the neutron diffraction data, but profile calculations using typical instrumental parameters suggest the resolution is sufficient to detect the second hydrogarnet phase. It is possible that the Sr-rich compound forms on the surface of the crystallites and is consequently more dominant in the XRD patterns. More likely, the products formed by reaction with D_2O have different profiles than those formed by reaction with H_2O. This observation is worthy of further studies.

Precise lattice parameters for the observed hydrogarnet phases were obtained by analysis of the synchrotron diffraction data and these are illustrated in Fig. 5. For a limited number of samples a third hydrogarnet phase was also observed. Interestingly, this was evident in the apparently less crystalline samples and it appears that the observed peak broadening is a consequence of the compositional inhomogeneity, rather than size or stain effects. The lattice parameter for the main phase in each composition displays a simple relationship with composition, but with noticeable deviation from Vegards law at low Sr levels. Other than for these compounds the lattice para-

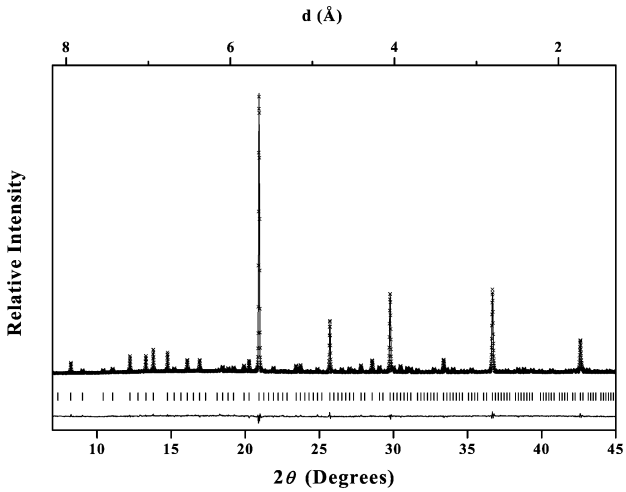

Fig. 4. Observed, calculated and differences diffraction patterns for the synchrotron powder XRD data of $Ca_{1.5}Sr_{1.5}Al_2O_6$. The pattern clearly demonstrates the sample is in single phase. The format is similar to Fig. 2.

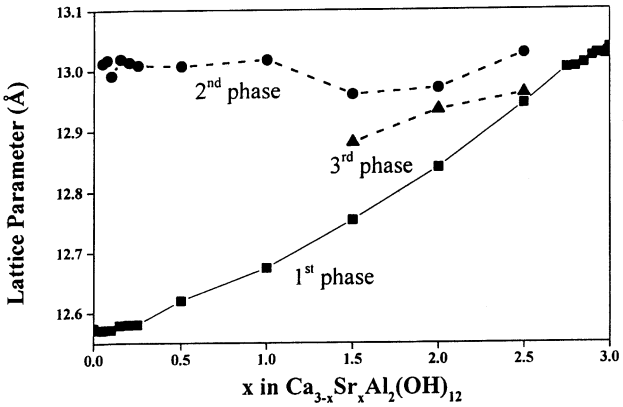

Fig. 5. Variation of a vs. composition for the series of hydroxides $Ca_{3-x}Sr_xAl_2(O_4H_4)_3$ hydrated for 2 weeks.

meter variations could be reasonably fitted by the quadratic $a = 12.56549 + 0.09437x + 0.02137x^2$.

In addition to giving precise lattice parameters, the Rietveld refinements also provided an estimate of the Ca/Sr ratio in each of the phases. The plot of calculated Sr occupancy vs. a confirms that the observed increase in lattice parameters is due to an increase in Sr content, although there is noticeable variation at intermediate contents, which is where the crystallinity of the samples is lowest. Fig. 6 also shows the theoretical Ca/Sr ratio and indicates that in all samples the observed Sr content in the crystalline phases is less than predicated from the stoichiometry of the starting oxide. This figure clearly illustrates that there is no miscibility gap and the entire collection of solid solution exists.

Despite the tendency for the segregation of the hydrogarnets, the high quality of the diffraction data has enabled us to refine reasonably precise structures, and thus identify any trends in the structures. Considering initially the neutron diffraction studies, we find that the mixed metal deuteroxides display similar O–H/D distances to those of the pure end-members. Indeed, Lager et al. [6] have previously described the hydrogarnet structure in relationship to the structure of grossularite because both contain OH_4 tetrahedra. The shortest intermolecular distances are around 2.575(4) Å, and are comparable to the sum of the van der Waals radii for H and O (2.69 Å) demonstrating H-bonding not to be important in these deuteroxides.

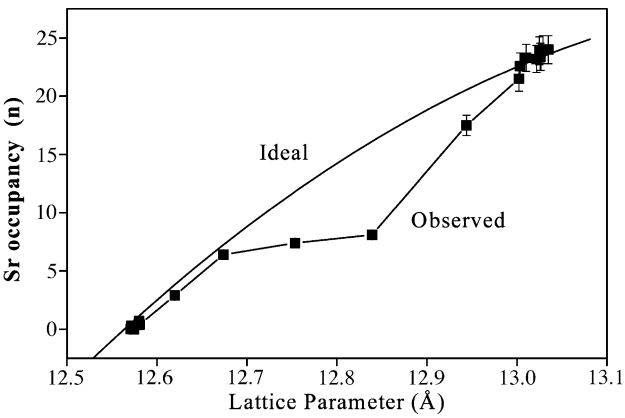

Fig. 6. Variation of occupancy vs. a for the series of hydroxides $Ca_{3-x}Sr_xAl_2(O_4H_4)_3$ hydrated for 2 weeks.

While being less precise than the structures refined from neutron diffraction data, the synchrotron refined structures are more revealing. The hydrogarnet structure consists of four asymmetric units, the disordered Ca/Sr cations occupying one site within a distorted cube. These cations are displaced so that there are four short and four somewhat longer M–O distances. The Al has an approximately octahedral environment (Fig. 7). In general, the Al–O distance increases slightly as the Sr content (and lattice size) increases, the variation is however relatively small, the distance increases from 1.910(2) to 1.945 Å. There is some scatter in refined Al–O distances in the samples with intermediate Ca/Sr compositions.

The changes in the AlO_6 octahedra are inducted by the expansion of the MO_8 moiety. The short M–O distance is 2.459(2) Å in $Ca_3Al_2(O_4H_4)_3$ and increases to 2.569(4) Å in $Sr_3Al_2(O_4H_4)_3$. The longer M–O distance increases from 2.521(2) to 2.659(4) Å over the same composition range. These values are in excellent agreement with value reported previously from powder neutron diffraction studies and illustrate the accuracy and precision obtainable with high-quality synchrotron diffraction data. The complexity of the materials obtained at intermediate compositions limited the precision of the structural refinements.

During the hydration of the oxides, $Ca_{3-x}Sr_xAl_2O_6$ vessels were not thermostated and the temperature of the reactions was observed to fluctuate between ca. 19 and 29 °C, i.e., where the hydrogarnet should form. Periodic

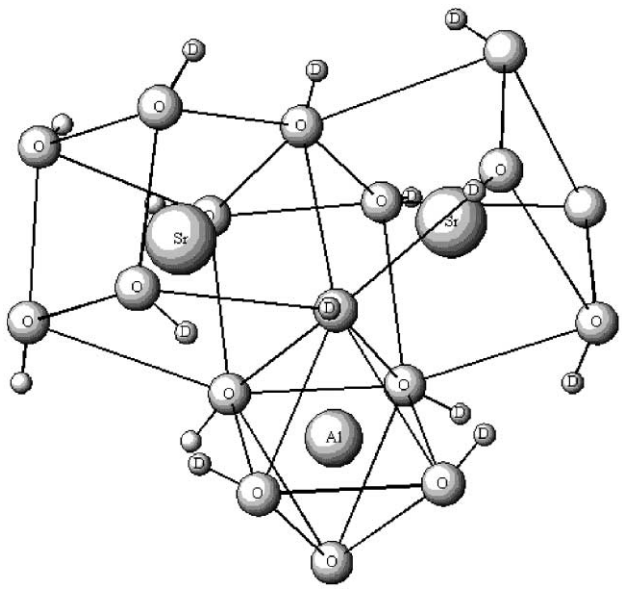

Fig. 7. Representation of octahedra AlO_6 and the dodecahedra.

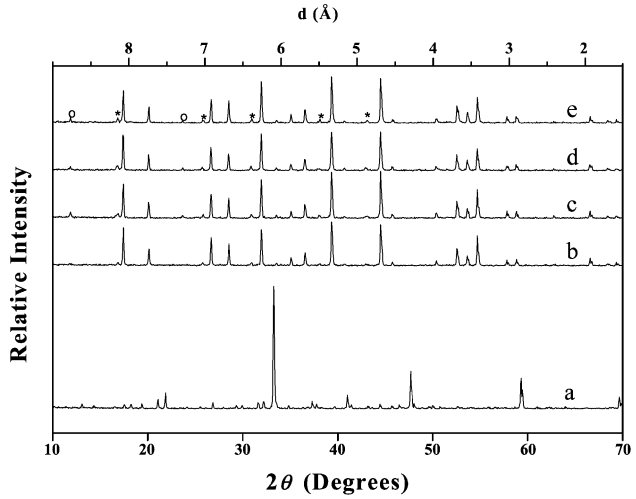

Fig. 8. Powder XRD patterns of the product formed after reaction of $Ca_{2.9}Sr_{0.1}Al_2O_6$ with water for (a) 0, (b) 1 day, (c) 3 days, (d) 1 week and (e) 2 weeks. The peaks labelled * indicate the presence of $Ca_{3-x}Sr_xAl_2(O_4H_4)_3$ ($x \approx 3$), while peaks with ° indicate $Ca_2Al_2O_5{\cdot}8H_2O$.

checks by XRD showed that the reaction was essentially complete after 1 day and further reaction produced small amounts of $Ca_2Al_2O_5{\cdot}8H_2O$. It was also observed that the amount of the Sr-rich $Ca_{3-x}Sr_xAl_2(O_4H_4)_3$ phase formed did not significantly alter on prolonged reaction (Fig. 8). These results suggest that the phase segregation is inherent to the hydration of these mixed metal aluminates.

The present results have confirmed and expanded upon Carson's initial observation of phase segregation in the $Ca_{3-x}Sr_xAl_2(O_4H_4)_3$ series. The most striking result is the formation of two or three phases from the single-phase starting oxides, suggesting these may be a miscibility gap in the $Ca_3Al_2(O_4H_4)_3$–$Sr_3Al_2(O_4H_4)_3$ series. This suggestion is in conflict with the observed formation of a number compounds with variable Ca/Sr ratios in this series. The third puzzle in the series is that once formed the mixed metal hydroxides are stable and there is no suggestion of Ca/Sr exchange.

In endeavouring to explain these observations, it is important to note that despite the apparent simplicity of the two structures, $Ca_3Al_2O_6$ is in space group $Pa\bar{3}$ with $a = 15.2745(5)$ Å and $Ca_3Al_2(O_4H_4)_3$ is in space group $Ia3d$ with $a = 12.5744(2)$ Å; the hydration reaction is not a topotatic reaction. Indeed, our studies have shown that there is a complex distribution of Ca and Sr over the available sites in $Ca_{3-x}Sr_xAl_2O_6$ [12]. This distribution is not present in the hydrated materials where a single Ca/Sr site exists. Studies of the early stages of hydration of $Ca_3Al_2O_6$ have revealed the presence of both an intermediate phase, and importantly, an induction period [16]. We postulate that the reaction proceeds by dissolution of the oxide and at a crucial concentration precipitation of the corresponding hydroxide. Given the solubilities of the Ca and Sr compounds are likely to be different (in general Ca salts are more soluble), precipitation of the Sr hydroxide will commence prior to that of the Ca hydroxide. Alternatively, given Ca and Sr occupy different positions in the $Ca_{3-x}Sr_xAl_2O_6$ lattice, it is possible that a reaction at an Sr-rich phase is favored, preferentially leaching this into solution and favoring precipitation of the Sr-rich hydroxide.

Irrespective of the mechanism by which Sr segregation occurs, the major point for Portland cements is that it does occur. This suggests that even when incorporation of impurity cations into the lattices of the starting oxides is possible, the impurity cations may not exist as a solid solution in the hydrated material. Indeed, due to segregation of these into separate phases, the impurity cations may be susceptible to leaching or other undesirable reactions.

4. Conclusion

The present high resolution studies confirm the early observation of Carlson [8] that hydration of the mixed Ca/Sr aluminates of the type $Ca_{3-x}Sr_xAl_2O_6$ produces a mixture of hydrogarnet phases. Refinements of the structures of the phases present in these products demonstrate that the series of solid solutions can exist and the segregation into Ca-rich and Sr-rich products is possibly related to differences in the solubility of the two products. It is now well established that the addition of various cations to form solid solutions with $Ca_3Al_2O_6$ can alter the behaviour of this phase [17], and it has been postulated that this could provide a method to immobilise toxic heavy metals [18]. The present work shows that hydration of $Ca_3Al_2O_6$ does not necessarily produce single-phase products and this phase is possibly unsuitable to immobilise heavy metals. Studies with other metals and phases in Portland cement are in progress.

Acknowledgments

This work was supported by the Australian Institute of Nuclear Science and Engineering. The synchrotron measurements at the Australian National Beamline Facility were supported by the Australian Synchrotron Research Program, which is funded by the Commonwealth of Australia under the Major National Research Facilities program.

References

[1] C.S. Poon, C.J. Peters, R. Perry, Use of stabilization processes in the control of toxic wastes, Effluent Water Treat. J. (November).
[2] M.A. Gülgün, O.O. Popoola, W.M. Kriven, Chemical synthesis and characterization of calcium aluminate powders, J. Am. Ceram. Soc. 77 (1994) 531–539.
[3] E. Breval, Gas-phase and liquid-phase hydration of C3A, Cem. Concr. Res. 7 (1977) 297–303.
[4] N. Richard, N. Lequeux, P. Boch, Local environment of Al and Ca in

CAH_{10} and C_2AH_8 by X-ray absorption spectroscopy, Eur. J. Solid State Inorg. Chem. 32 (1995) 649–662.
[5] P. Mondal, J.W. Jeffery, The crystal structure of tricalcium aluminate, $Ca_3Al_2O_6$, Acta Crystallogr. B 31 (1975) 689–697.
[6] G.A. Lager, T. Armbruster, J. Faber, Neutron and X-ray diffraction study of hydrogarnet $Ca_3Al_2(OH)_{12}$, Am. Mineral. 72 (1987) 756–765.
[7] N. Bouzoubaâ, M.H. Zhang, A. Bilodeau, V.M. Malhotra, Laboratory-produced high-volume fly ash blended cements: Physical properties and compressive strength of mortar, Cem. Concr. Res. 28 (1998) 1555.
[8] E.T. Carlson, A study of some strontium aluminate and calcium–strontium aluminate solid solutions, J. Res. Natl. Bur. Stand. 54 (1955) 2334–2595.
[9] B.C. Chakoumakos, G.A. Lager, J.A. Fernandez-Baca, Refinement of the structures of $Sr_3Al_2O_6$ and the hydrogarnet $Sr_3Al_2(OD)_{12}$ by Rietveld analysis of neutron powder diffraction data, Acta Crystallogr. C. 48 (1992) 414–419.
[10] L. Walz, Pulverdiffraktometrische untersuchungen am system $Sr_{3-x}Ca_xAl_2O_6$ sowie einkristallstrukturnalysen für di fälle $x=1{,}359(8)$, 1,62(1) und 2,12(1), Z. Kristallogr. 213 (1998) 47–51.
[11] A.K. Prodjosantoso, B.J. Kennedy, B.A. Hunter, Synthesis and structural studies of strontium-substituted tricalcium aluminate $Ca_{3-x}Sr_xAl_2O_6$, Aust. J. Chem. 53 (2000) 195–202.
[12] H.M. Rietveld, A profile refinement method for nuclear and magnetic structures, J. Appl. Crystallogr. 2 (1969) 65–71.
[13] B.A. Hunter, C.J. Howard, A Computer Program for the Rietveld Analysis of X-ray and Neutron Powder Diffraction Patterns, Australian Nuclear Science and Technology Organisation, Menai, NSW, 1996.
[14] G. Caglioti, A. Paoletti, F.P. Ricci, Nucl. Instrum. 2 (1958) 233.
[15] V.F. Sears, Atomic Energy of Canada Limited Report AECL-8490, 1984.
[16] A.C. Jupe, X. Turrillas, P. Barnes, S.L. Colston, C. Hall, D. Hausermann, M. Hanfland, Fast in situ X-ray-diffraction studies of chemical reactions: A synchrotron view of the hydration of tricalcium aluminate, Phys. Rev. B 53 (1996) 14697–14700.
[17] My.Y. Benarchid, A. Diouri, A. Boukhari, J. Aride, R. Castanet, J. Rogez, Thermal study of chromium–phosphorus-doped tricalcium aluminate, Cem. Concr. Res. 31 (2001) 449–454.
[18] T.E. Mayers, M.E. Eappi, Laboratory evaluation of stabilization/solidification technology for reducing the mobility of heavy metals in New Bedford Harbor superfund site sediment, Stabilization of Hazardous Radioactive and Mixed Wastes, second ed., ASTM Publication, Philadelphia, PA, 1992, p. 304.